



Enhancing material removal processes using modulation-assisted machining

J.B. Mann^{a,b}, Y. Guo^a, C. Saldana^{a,b}, W.D. Compton^a, S. Chandrasekar^{a,*}

^a Center for Materials Processing and Tribology, School of Industrial Engineering, 315 N. Grant St., Purdue University, West Lafayette, IN 47907, USA

^b M4 Sciences LLC, 1201 Cumberland Avenue, Suite A, West Lafayette, IN 47906, USA

ARTICLE INFO

Article history:

Received 15 September 2010

Received in revised form

18 May 2011

Accepted 20 May 2011

Available online 30 May 2011

Keywords:

Machining

Chip

Wear

Texture

ABSTRACT

The controlled application of low-frequency modulation to machining – Modulation Assisted Machining (MAM) – is shown to effect discrete chip formation and disrupt the severe contact condition at the tool–chip interface. This enables chips of different morphologies, including discrete-particle like chips, to be created, and prescription of the machined surface texture. A model for MAM is used to describe chip formation regimes and textures. Benefits include improved chip management; enhanced lubrication; reduction of tool wear; and enhanced material removal rates. Prototype implementation of MAM in processes such as drilling and turning is described in case studies.

© 2011 Elsevier Ltd. All rights reserved.

1. Introduction

The mechanics of material removal in machining-based processes such as turning, drilling and boring is unique in many respects. First, the formation of a continuous chip is an intrinsic characteristic of the material removal in machining of ductile metals and alloys. However, continuous chips pose a hurdle to enhancing machining performance because of issues associated with chip evacuation, interference with tooling, and lubrication of the tool–chip contact [1]. For example, in deep-drilling processes, the drilling performance, e.g., removal rate, tool life, is often determined by the rate at which the continuous chips can be evacuated from inside the drilling zone, which lies deep inside a hole. Similar issues are present in high-rate turning and boring. It is often not realized that an important reason for application of fluid at high-pressure and flow-rate, so typical of many machining systems, is to break continuous chips into smaller, more easily manageable fragments and evacuate them from the machining zone. The use of high volumes of fluid for such ‘secondary purposes’ as chip management is less than desirable given the high burden that is attached to use of Metal Removal Fluids (MRFs) in terms of cost (up to 16 percent of total machining costs in some operations), infrastructure demands and impact on health and the environment [2].

Second, the tool–chip interface in continuous chip formation represents an extreme tribological condition characterized by contact between pristine surfaces under conditions of high

normal and shear stresses, and elevated temperatures. Over much of the contact, the real and apparent areas are essentially equal – the so-called region of intimate contact [1,3–5] – making it difficult for a fluid to penetrate the contact. Thus it is difficult to lubricate the contact, with fluid action typically being confined to the very edges of the contact [1,4,6–8]. In contrast, conventional sliding or rolling contacts, characterized by the real area of contact being a small fraction (~ 1 percent) of the apparent area, are usually well-lubricated [1]. Direct observations of the tool rake face made *in situ* during cutting using optically transparent sapphire tools have shown the contact region to be composed of two distinct zones. A zone of intimate contact extends from the cutting edge to some distance up the rake face wherein the real and apparent areas are equal, followed by a zone of intermittent (disrupted) contact with metal deposits that extends to the edge, where the chip separates from the tool (Fig. 1a) [4,5]. When a fluid is applied to the machining zone, the region of metal deposits disappears (Fig. 1b) indicating that the fluid is active along the edges of the chip–tool contact. Observations carried out using luminescence and high-speed photography methods, however, show little evidence of fluid penetration into the intimate contact region [8], which is also consistent with other indirect inferences of the cutting zone [1,3,6]. The friction conditions in the intimate contact region determine the tool–chip contact temperature, type and rate of tool wear, and the energy consumption in machining. For example, thermo-chemical wear mechanisms play a major role in determining tool life in machining processes [9]. Common examples of thermo-chemical wear include the rapid wear of diamond tools when machining ferrous materials, and cubic boron nitride tools when machining compact graphite iron (CGI) [1,9,10]. Furthermore, since about 30 percent

* Corresponding author. Tel.: +1 7654943623; fax: +1 7654945448.
E-mail address: chandy@ecn.purdue.edu (S. Chandrasekar).

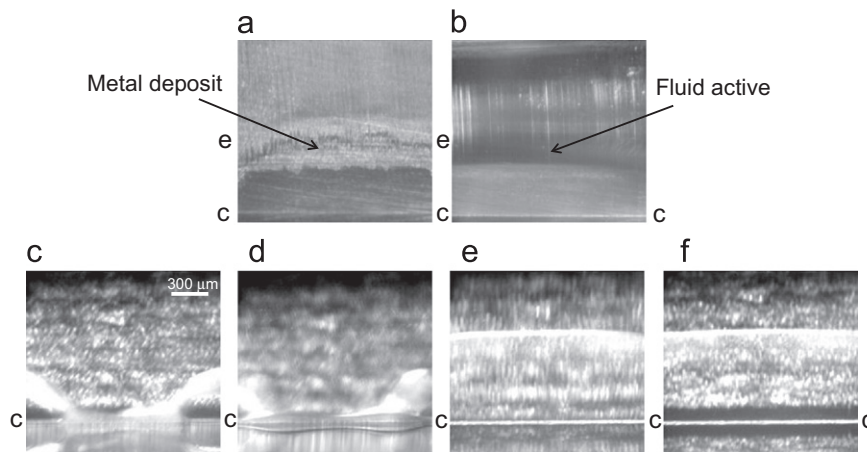


Fig. 1. Direct images of rake face (tool–chip contact) of sapphire tool selectively extracted from a high-speed photographic sequence of 2-D linear machining showing (a) conventional dry machining; (b) conventional machining with fluid; and (c)–(f) machining with velocity-modulation in presence of a fluid. Note that in (b), fluid is active in the intermittent contact region disrupting formation of metal deposits but it does not appear to enter the intimate contact region. In the modulation machining, chip–tool contact is just broken in (c) resulting in fluid entering the contact. The contact is then re-established in (e) with cutting continuing on in (f). Fluid appears to be present over much the contact during this modulated cutting except in the black band immediately adjoining the cutting edge (f). The images were taken in low speed cutting ($V < 10$ mm/s) Modulation frequency $f_m = 12.5$ Hz, modulation amplitude $A = 200$ μm , tool rake angle 5° . ‘cc’ is the cutting edge and ‘ee’ is the edge of the tool–chip contact.

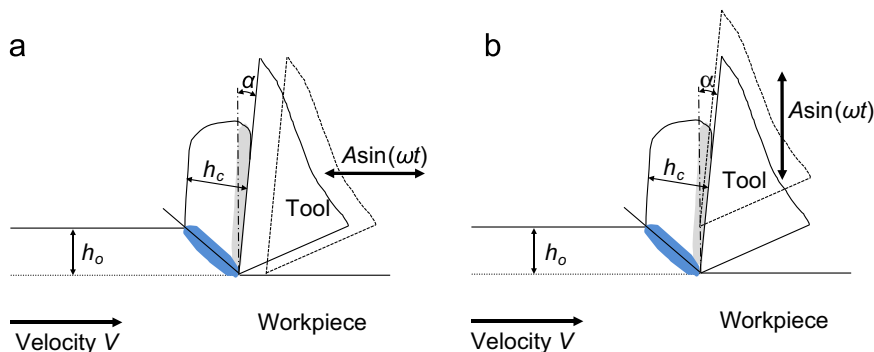


Fig. 2. Schematic of machining with superimposed modulation (a) velocity-modulation and (b) feed-modulation. V is the mean (steady) cutting velocity, h_o is the undeformed chip thickness (feed/rev in turning), and ω is $2\pi f_m$, where f_m is the frequency of modulation. The darker and lighter shaded areas indicate the regions of primary and secondary shear deformation, respectively.

of the specific energy of machining is dissipated by friction in the intimate contact zone, the lack of effective fluid action therein is an important contributor to the high energy consumption in machining.

A third unusual characteristic of continuous chip formation is that the chip material during removal is subject to very large plastic strains quite atypical of conventional deformation processes. These strains, another major reason for the large specific energies recorded in machining, are also in part determined by the severity of the tool–chip contact condition [1,9,11].

These characteristics of machining suggest that if material removal with ductile alloys can be effected by ‘discrete chip formation’ rather than the typical continuous chip, and the severity of the contact condition at the tool–chip interface can be disrupted to facilitate enhanced fluid action, then the performance of machining processes assessed in terms of chip management, tool wear, energy consumption and fluid usage, can be enhanced significantly. It is shown herein that machining with a controlled low-frequency modulation (< 1000 Hz) – Modulation-Assisted Machining (MAM) – effects discrete chip formation and disrupts the severity of the tool–chip contact in a controlled manner with attendant benefits. Furthermore, because of the additional degrees of freedom offered by the modulation, MAM can be used for surface texturing and for production of powder particulate, potentially creating new application domains for

machining. From a viewpoint of implementation, MAM can be incorporated in industrial machining systems with minimal equipment modifications.

2. Background

It is difficult to place the first known application of a controlled modulation or vibration to machining processes. There is certainly a discussion of consequences of ‘chatter vibration’ on chip formation in the 1950s [12,13]. A patent by Findley [14] gives detailed consideration of modes of application of vibration to machining processes and some of its consequences for chip formation. However, the underlying scientific details pertaining to the mechanics of chip formation and tool–chip contact receive less than adequate consideration. The major body of work on use of controlled vibration to ‘assist’ machining processes, though mainly in the ultrasonic regime, appears to have emerged from the studies of Kumabe [15]. Specifically, the application of the modulation can be classified into two types, each with fundamentally different kinematics: (a) modulation in the direction of cutting velocity—velocity-modulation (Fig. 2a) and (b) modulation in the direction of tool-feed or undeformed chip thickness—feed-modulation (Fig. 2b).

Fig. 2a shows a schematic of plane-strain machining with sinusoidal velocity-modulation. The cutting velocity varies continuously during each cycle of modulation in this configuration. In particular, the direction of instantaneous velocity is reversed and the tool–chip contact is completely disrupted, during each cycle of modulation, when the superimposed modulation velocity exceeds the mean (steady) cutting velocity. This corresponds to $\omega A > V$, where ω is the angular modulation frequency and $2A$ is the peak-to-peak amplitude. In practice, ωA may need to be set slightly greater than V to achieve this disruption because of the compliance of the system. This disruption of the tool–chip contact for $\omega A > V$ has been confirmed in the low frequency regime in specially devised cutting experiments wherein a linear motor was used to impose the steady cutting speed as well as the modulation [16,17]. The experiments also showed that in the absence of the modulation (conventional machining), the tool and chip were found to be in intimate contact with little visible penetration of a fluid (externally applied) into this contact region [8,16], see also Fig. 1b. However, in the presence of a modulation sufficient to disrupt the contact, there was visible penetration of the fluid over the entire contact region, as revealed by high-speed photography of the contact (Fig. 1c–f), and confirmed also by other less direct observations [16,18]. This penetration of fluid into the contact typically coincided with a substantial, often 2–3 fold, reduction in the ‘friction coefficient’ (i.e., ratio of tangential to normal force on tool rake face) at the contact [16,18]. An interesting demonstration of velocity-oriented modulation machining, albeit in the ultrasonic modulation (high frequency) regime, is diamond turning of steel at relatively low workpiece speeds (0.02–0.07 m/s) [19]. In conventional machining, this process is characterized by excessive tool wear because of the high chemical affinity between iron and diamond. Disruption of the severity of the tool–chip contact and smaller interfacial temperatures, which reduce the propensity for thermo-chemical interactions, have been cited as the reasons for the success of this application of modulation [19].

While the velocity-modulation is effective at disrupting the severity of the tool–chip contact to enhance lubrication, reduce frictional dissipation and, potentially, lower the contact temperature [16,19], this approach has inherent limitations. The disruption condition of $\omega A > V$ is difficult, if not impossible, to realize in practice even at ultrasonic frequencies, except at the very low end of industrial machining speeds ($V < 0.5$ m/s). This is a consequence of dynamic system level constraints [15,19,20]. Furthermore, this type of modulation does not result in the formation of discrete chips, since the undeformed chip thickness is essentially constant throughout the cutting process (Fig. 2a). And, lastly, this modulation is kinematically difficult to impose in processes such as drilling and boring, which would require a superimposed oscillation in the rotation direction [20]. Of more general applicability is the use of feed-modulation of low frequency, wherein discrete chip formation and disruption of the tool–chip contact can be concurrently realized even at machining speeds ($V \gg 0.5$ m/s) typical of practice. This is the modulation configuration of interest to the present study.

3. Geometry and mechanics of MAM

Fig. 2b shows a schematic of plane-strain machining with sinusoidal modulation, $A \sin(2\pi f_m t)$, superimposed in a direction parallel to the undeformed chip thickness (i.e., tool feed in turning or drilling) on to the continuous linear motion of a tool. This configuration will henceforth be referred to as MAM. The cutting speed is unaffected by modulation; however, the modulation imparts a sinusoidal velocity of magnitude $2\pi f_m A \cos(2\pi f_m t)$ oriented in the direction of undeformed chip thickness. Unlike

conventional machining ($f_m = 0$ or $A = 0$), the instantaneous undeformed chip thickness is not constant but varies with time (t) between some maximum and minimum value as $h(t) = h_o + A \sin(2\pi f_m t)$, where h_o is the undeformed chip thickness in the absence of the modulation. This is under the assumption that the initial surface over which the tool makes the cutting pass is flat, as shown in Fig. 2b. It is evident that if A is sufficiently large and in excess of some critical value, then $h(t)$ becomes less than or equal to zero during each cycle of modulation, resulting in ‘discrete chips’, these being produced at the rate of f_m per second. Also, at this condition, the tool–chip contact is disrupted f_m times per second [20,21].

The critical value of the modulation amplitude (A) needed to realize discrete chip formation can be estimated for general machining configurations involving continuous cutting (e.g., turning, linear machining) based on consideration of the motion of the tool. Consider lathe turning, for example, where a workpiece of diameter, d , is rotating at a frequency, f_w , and material is removed by feeding the tool at a rate of h_o per revolution in a direction parallel to the axis of rotation. For analysis of tool motion *per se*, this turning can be transformed into 2-D machining by unwrapping each revolution of the cylindrical workpiece surface onto a plane surface (Fig. 3). A Cartesian frame of reference is established with the x -axis along the circumferential (velocity) direction and the y -axis along the axial (feed) direction. The cutting is then realized by 2-D motion of the tool in the x - y plane as in Fig. 3. Each revolution of the cylindrical workpiece is now transformed into one complete cycle of cutting across the plane from $x = 0$ to $x = \pi d$ (i.e., the workpiece circumference) with the subsequent cycle beginning again at $x = 0$ and proceeding along the y -axis. If a sinusoidal feed-modulation of amplitude A and frequency f_m is now superimposed, then the position of the tool during the n th cycle can be described as (Fig. 3) [22]

$$y_n(x) = (n-1)h_o + h_o x / (\pi d) + A \sin(2\pi x / \lambda + (n-1)\phi), \quad 0 \leq x \leq \pi d \quad (1)$$

$$\lambda = \pi d f_w / f_m \quad (2)$$

$$\phi = 2\pi(f_m / f_w - \text{INT}[f_m / f_w]), \quad 0 \leq \phi < 2\pi \quad (3)$$

where λ is the spatial wave length of the sinusoidal path and ϕ is a measure of the phase difference ($0 \leq \phi < 2\pi$) between two consecutive cycles (Fig. 3). In Eq. (3), ‘INT[]’ denotes the integer part of the value.

When the tool does not completely disengage from the workpiece during any portion of a path, then any two consecutive paths of the tool, $y_n(x)$ and $y_{n-1}(x)$, will not intersect. Fig. 3 shows one of such example. The undeformed thickness of the chip at any

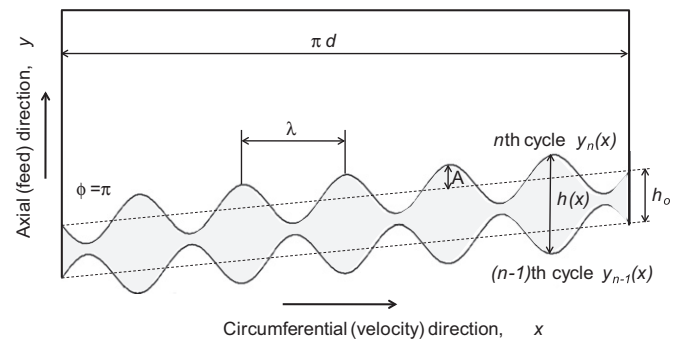


Fig. 3. 2-D model of geometry in cylindrical turning with modulation amplitude, A . Two successive cycles or traverses of the tool are shown on the unfolded cylinder surface with the shaded region between them representing the undeformed chip thickness, $h(x)$.

stage of the cutting is then obtained simply as

$$h(x) = y_n(x) - y_{n-1}(x) \tag{4a}$$

Indeed, the shaded region in Fig. 3 defines the geometry of the undeformed chip. More generally, the undeformed chip thickness at steady state can be represented succinctly as

$$h(x) = y_n(x) - \max_i(y_i(x)), \quad i = 1, 2, \dots, n-1 \tag{4b}$$

which takes into account the cumulative effect of the prior cutting paths in determining the steady state profile of the machined surface.

The minimum amplitude for effecting discrete chip formation is obtained by setting $h(x)=0$ in Eq. (4). By incorporating Eqs. (1)–(3) into Eq. (4), it may be shown that this minimum amplitude, in non-dimensional form, is given by

$$A/h_o = 1/[2\sin(\phi/2)] \tag{5}$$

Fig. 4a shows this dependence of A/h_o on ϕ in graphical form. Since ϕ depends only on f_m/f_w (Eq. (3)), A/h_o can also be plotted as a function of f_m/f_w as in Fig. 4b; in this latter framework, the single curve of Fig. 4a decomposes into multiple curves. The principal characteristics of chip formation in MAM can be analyzed using Fig. 4a. The U-shaped curve shown in the figure marks the boundary between continuous cutting (i.e., $h(t) > 0$) and discrete cutting, where MAM conditions cause the undeformed chip thickness calculated in Eq. (4) to periodically become equal to or less than zero (mathematically $h(t) \leq 0$, but physically the undeformed chip thickness $h(t)=0$). Thus, the curve demarcates two distinct cutting regimes. For MAM conditions outside the U-curve (shaded area), the tool is always engaged with the workpiece and cutting is continuous, despite the superimposed oscillation on the machining. MAM conditions inside the curve (unshaded area) result in discontinuous cutting with discrete chip formation, as well as disruption of the tool–chip contact in each cycle of modulation. Points along the U-curves in Fig. 4a and b, represent the minimum modulation amplitude required to effect discrete chip formation (i.e., $h(t)=0$) at the respective values of f_m/f_w . The global minimum or smallest value of A for discrete chip formation is given by $2A=h_o$ and occurs when $\phi=\pi$; this value of ϕ corresponds to $f_m/f_w=1/2(2N+1)$, where N is an integer (Fig. 4 and Eq. (5)). This modulation condition, with $f_m/f_w=1/2(2N+1)$ and peak-to-peak amplitude, $2A=h_o$, has been labeled as the optimum modulation condition [17,18]. At other values of this frequency ratio, the minimum peak-to-peak amplitude, $2A$, for discrete chip formation is greater than h_o . Eq. (5) and Fig. 4 also show specific instances, where the conditions of modulation are not sufficient to realize discrete chip formation. At the asymptotic ends of each of the U-curves corresponding to $f_m/f_w=N$, successive cutting cycles are ‘in phase’ and discrete chip formation is never realized

regardless of the magnitude of A . Instead, a continuous chip of constant thickness should be expected to form at all machining conditions when the ratio f_m/f_w is an integer.

Amplitude-frequency conditions for describing chip formation with tools having multiple cutting edges, such as in drilling, can be established in an analogous way. It will suffice to state here that for a tool with k cutting edges, Eq. (5) and Fig. 4 can still be used to demarcate the boundary between the discrete and continuous cutting regimes if f_w is replaced everywhere in the equation (and the figure) by kf_w and h_o by h_o/k . The optimum modulation condition for this case then becomes $2A=h_o/k$ with $f_m/f_w=k(2N+1)/2$.

It is of interest to highlight some of the applications-related aspects of the kinematics of MAM. Eq. (5) indicates that the amplitude condition for discrete chip formation and tool–chip contact disruption can be realized even at high cutting speeds [18,20], in contrast to the velocity-modulation case. For example, since amplitudes as large as 0.2 mm can be achieved using piezo-type actuators in low-frequency modulation ($f_m < 1000$ Hz), MAM is capable of effecting discrete formation even at cutting speeds of ~ 1000 m/min. This makes feed-modulation especially well-suited for implementation at the cutting speeds typical of industrial practice. Conditions for enhancing fluid action in the intimate contact region can, potentially, thus be realized even at such extreme speeds. Furthermore, the overall material removal rate (MRR) in MAM is determined only by the machining conditions and not affected by the modulation parameters. That is, the mere superimposition of the modulation to the machining, while effecting discrete chips, does not change the MRR which is already prescribed by the baseline machining parameters.

Eq. (5) and Fig. 4 provide guidelines for setting the amplitude–frequency conditions to effect discrete chip formation. In general, the minimum amplitude (optimum) condition is to be preferred, unless process constraints on f_m and A warrant otherwise. Of course, in practice, to achieve discrete chips, the modulation amplitude may have to be set somewhat higher than the minimum values predicted by Eq. (5) to compensate for system compliance, a factor not considered in the analysis leading to Eq. (5). With regard to selection of the specific f_m/f_w ratio for discrete cutting (Fig. 4b), it may generally be preferable to use the larger values of this ratio, as this would cause the chip formation to be interrupted more frequently, resulting in smaller discrete chips and improved lubrication of the contact. Indeed, high values for this ratio result in very short, fiber-like chips, an aspect exploited in production of particulate and fibers by MAM [21]. However, the largest f_m/f_w ratio achievable in practice will be determined by the maximum amplitude that the modulation device can provide at a particular modulation frequency. Lastly,

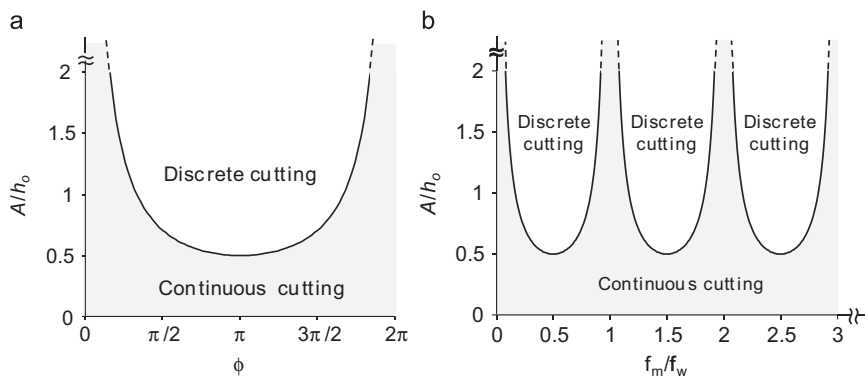


Fig. 4. Cutting regimes of MAM in (a) $\phi - A/h_o$ space and (b) $f_m/f_w - A/h_o$ space. The transition from continuous cutting to discrete cutting occurs across the U-curves.

to avoid rubbing between the tool flank and the freshly generated surface, the tool clearance angle has to satisfy a constraint that is generally met in practice [22].

4. Verification of chip formation characteristics

A series of 2-D turning experiments was carried out with a single-edge ($k=1$), high-speed steel cutting tool to verify the chip formation characteristics predicted in MAM (Eq. (5) and Fig. 4). A commercial modulation device (M4 Sciences LLC) mounted onto the turret of a CNC lathe, was used to impose the feed modulation (Fig. 5). This device is compact and easily incorporated into the

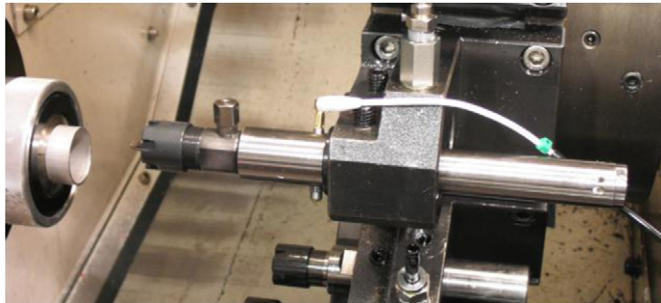


Fig. 5. Commercial modulation device used in the turning experiments to verify chip formation characteristics, and in the drilling experiments corresponding to Tests 1–7. The left hand side of the image also shows the aluminum tube workpiece used in the turning experiments.

machining system. The device employs a piezo-electric actuator to impose the modulation with amplitudes of up to 0.2 mm at frequencies up to 1000 Hz [20]. This system allows for the use of modulation in machining processes that cover a wide range of industrial conditions. Since the modulation is applied locally at the cutting tool, the system eliminates dynamic and inertia effects that cause complications when attempting to modulate machine slides with relatively large mass. The commercial system for modulation-assisted machining enables controlled experimental investigation over a range of modulation conditions.

The machining and modulation conditions were selected so as to explore the cutting regime spanned by one of the U-curves, specifically that centered around an optimum modulation condition of $f_m/f_w=5.5$ (Fig. 6). The machining conditions were: workpiece material, Al 6061T6 tube, 25.4 mm diameter and 1.2 mm wall thickness; $f_w=20$ Hz; $h_o=0.02$ mm/rev; depth (width) of cut=1.2 mm; and fluid, commercial vegetable based cutting oil (Blaser VascoMill™ 10). Approximately 40 modulation frequency conditions in the range of 100–120 Hz were studied (Fig. 6). The chips created at the different conditions were collected carefully on sheets of paper placed immediately under the cutting zone, cleaned with isopropyl alcohol and examined under an optical stereo microscope (Olympus model SZX9) to analyze their morphology (e.g., discrete, continuous, and shape).

Optical microscope pictures of the chips formed at select MAM conditions are shown in Fig. 6, together with the U-curve demarcating the discrete and continuous cutting regimes. The singular feature of this figure is confirmation of the predictions of chip formation in the two MAM regimes by the observed chip morphologies. In the discrete cutting regime, the chips are

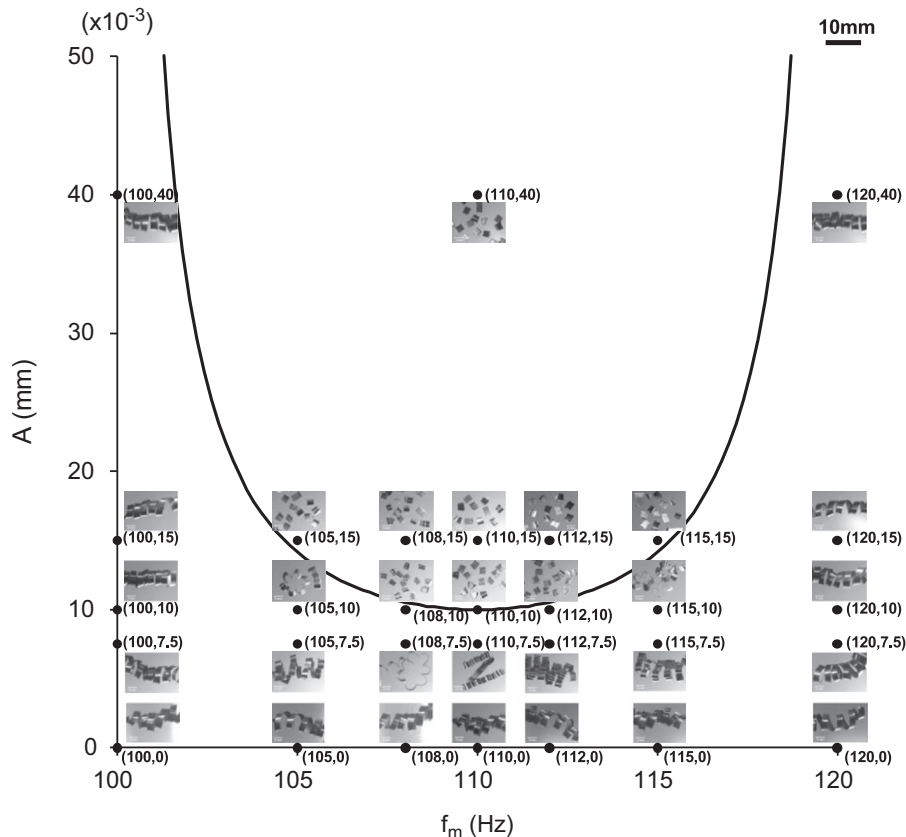


Fig. 6. Optical microscope pictures showing chip forms created at the various MAM conditions; machining conditions: $f_w=20$ Hz, $h_o=0.01875$ mm (feed/rev, machine setting), depth of cut=1.2 mm, $d=25.4$ mm. Note the close correspondence between predicted and observed chip formation at the modulation frequency and amplitude conditions tested (f_m, A). The chips corresponding to conventional machining ($A=0$) are shown in the bottom row.

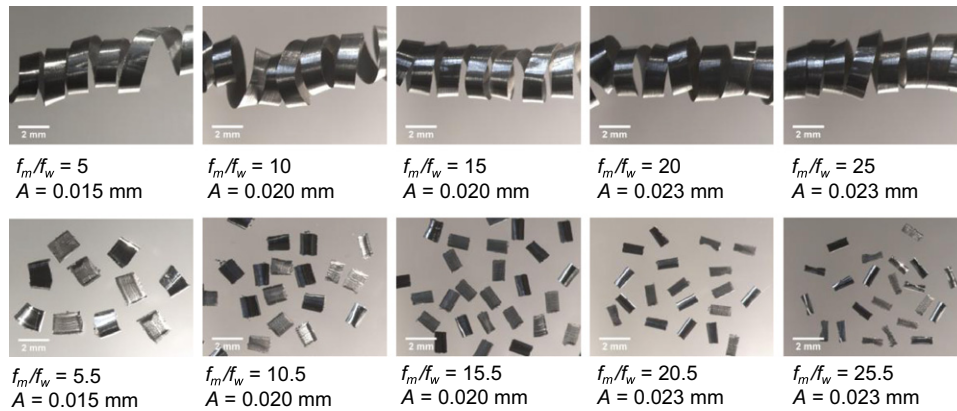


Fig. 7. Chips generated at increasing values of the ratio f_m/f_w ($f_w=20$ Hz). The top row corresponds to MAM conditions of continuous cutting and the bottom row to discrete cutting. All of the pictures are at the same magnification.

seen to be of much smaller size, than in the continuous cutting regime. The continuous cutting regime is characterized by longer, stringy chips more typical of conventional machining of this alloy. For reference, samples of chips from conventional machining ($A=0$) are shown in the bottom row of the figure. The results also show the effect of increasing modulation amplitude on the continuous chip formation. In Fig. 6, the images of chips created below the U-curve, with $A=0.0075$ mm, e.g., points (105, 7.5) (108, 7.5), (110, 7.5) (112, 7.5) and (115, 7.5), show a remarkable sinusoidal variation in chip thickness as expected from Eq. (4). Equally remarkable is the relatively sharp transition in the chip size observed when going across the U-curve in Fig. 6. It should be pointed out that the chips generated in the continuous cutting regime immediately adjoining the U-curve e.g., points (108, 10) and (112, 10), may appear similar to the chips in the discrete cutting regime. However, it was observed, both visually and using high-speed photography, that these chips formed (at this ‘near U-curve’ condition) in the cutting zone as longer fragments. However, they broke into smaller pieces soon after their formation due to the chip thickness in local regions of the chips being very small. Thus, this discreteness is an ‘apparent discreteness’ arising from the ‘geometric fragility’ of these chips. The chip formation analysis also predicts that at the asymptotes of the U-curve, continuous chips should always occur irrespective of the modulation amplitude. This is indeed seen to be the case in the experiments, even when the amplitude was set as high as four times the optimum amplitude required to effect discrete chips (Fig. 6). This confirms an earlier observation that the application of a modulation, even of very large amplitude, is in itself not sufficient to achieve discrete chip formation.

Predictions regarding the effect of modulation conditions on chip morphology were explored by fixing the modulation amplitude close to the optimum condition and varying f_m/f_w between 0 and 30. The bottom row of optical microscope pictures in Fig. 7 show chips obtained from these experiments for select f_m/f_w values in the discrete cutting regime. It is seen that as f_m/f_w is increased, the chip lengths become increasingly smaller, consistent with discrete chip segments being formed more frequently at the rate of f_m/f_w per revolution. Also, when f_m/f_w is set equal to integer values, continuous chips of constant thickness result as in the top row of pictures in Fig. 7. These observations are again consistent with predictions of the chip formation model for turning ($k=1$). Predictions of chip formation characteristics for tools with multiple cutting edges have likewise been verified using drilling ($k=2, 3$ (2- and 3-fluted drills)) and end milling ($k=4$) experiments.

5. Enhancing capability by discrete chip formation

A series of controlled MAM and conventional (baseline) machining tests using conditions typical of industrial applications (sometimes industrial case study conditions) was carried out to demonstrate the benefits, if any, arising from discrete chip formation and periodic disruption of the tool–chip contact. The configuration used in most of these tests was drilling with a 2-fluted drill, a prototypical machining process whose performance is often determined by the effectiveness of evacuation of chips from the machining zone deep inside a hole. The tests were specially designed using somewhat extreme machining conditions in order to evaluate performance parameters such as tool wear, material removal rate, cycle time and deep-drilling capability (in terms of length-to-diameter (L/D) of the hole). Details of the tests, whose outcomes are discussed in some detail, are presented in Table 1, with the bold face entries in the table representing the performance-related outcomes. As can also be seen from Table 1, the work materials used, e.g., stainless steels, Inconel® 718, Hastelloy® 625, were taken from a category that is often considered by industry to be difficult to machine. Typically, in these tests, the MAM used the same conditions as those employed in the baseline machining. The principal difference with MAM was in the use of modulation of specific amplitude and frequency, typically at or near an optimum modulation setting, to effect discrete chip formation and contact disruption.

Test 1 was designed to show that discrete chips of small length (deformed chip lengths in the order of $\sim D/10$) could be created by MAM even in highly ductile materials like stainless steel 316. A commonly encountered problem in drilling of these stainless steels is the generation of long continuous chips that pack the drill flutes causing failure of the drill and the drilling process. The flutes are the main passages through which drilling chips exit the drilling zone located deep inside a hole; in the present case hole L/D was up to 15. Test 2, involving drilling of Ti6Al4V, is an example showing that MAM can reduce the cycle time, in this case on average from 105 to 75 s. This was possible because a higher nominal feed rate (h_o) could be used when drilling with MAM – a consequence of its discrete-chip forming capability – than in the baseline machining. This is the only instance in Table 1, wherein a baseline machining condition was altered for the MAM test. Tests 3 and 4 highlight quite remarkable capability improvements with applications impact. In Test 3, the drills typically failed in the baseline tests even before completing one hole. In contrast, with MAM, failure did not occur even after drilling 5 holes. Test 4 shows a case where, with MAM, the typical life of the drill was extended to about 600 parts, in contrast to about 250 parts at the baseline

Table 1
Performance attributes of MAM and baseline machining.

Test no.	Attribute	Description	Tooling	Fluid	Workpiece	Baseline machining conditions	MAM conditions
1	Chip control	Drilling 5.0 mm dia, 75 mm deep hole	2 flute straight flute carbide tipped coolant fed drill	Oil, 80 bar	Stainless steel alloy 316	2400 RPM ($f_w=40$ Hz), 0.010 mm/rev, Long continuous chip	$f_m=200$ Hz, $A \approx 0.010$ mm, Discrete chips length $\sim D/10$
2	Cycle time	Drilling 3.5 mm dia, 105 mm deep hole	Single flute carbide coolant fed gun drill	Oil, 80 bar	Titanium alloy Ti6Al4V	4200 RPM ($f_w=70$ Hz), 0.015 mm/rev, 105 s drilling time	$f_m=105$ Hz, $A \approx 0.012$ mm, 0.020 mm/rev, 75 s drilling time
3	Extreme drilling feed rate	Drilling 5.05 mm dia, 75 mm deep hole	Single flute carbide coolant fed gun drill	Oil, 80 bar	Steel alloy 31CrMoV9	4800 RPM ($f_w=80$ Hz) 0.075 mm/rev < 1 hole to drill failure	$f_m=40$ Hz, $A \approx 0.050$ mm, > 5 holes drilled
4	Tool Wear	Drilling, 0.32 mm dia, 2.5 mm deep hole	2-flute carbide TiN coated high speed steel cobalt twist drill	Oil, flood	Steel alloy 4140	9660 RPM ($f_w=161$ Hz), 0.005 mm/rev, PECK CYCLE 0.150 mm/peck, 8 s drilling time, drill life ≈ 250 parts	$f_m=161$ Hz $A \approx 0.004$ mm, NO PECK CYCLE, 4 s drilling time, drill life ≈ 600 parts
5	Peck Drilling	Drilling 7.0 mm dia, 35 mm deep hole	2-flute TiAlN coated carbide coolant fed twist drill	Oil, 80 bar	Copper Alloy 101	4800 RPM ($f_w=80$ Hz), 0.100 mm/rev, PECK CYCLE, 1.5 mm/peck, 10 s drilling time	$f_m=240$ Hz, $A \approx 0.030$ mm, NO PECK CYCLE, 6 s drilling time
6	Drilling beyond flute	Drilling, 0.760 mm dia, 14.50 mm deep hole	2-flute uncoated carbide twist drill, 12.5 mm flute length	Oil, flood	Nickel alloy Inconel [®] 718	4020 RPM ($f_w=67$ Hz) 0.005 mm/rev, 0.125 mm/peck, 24 s drilling time, Drilling beyond flutes caused drill failure	$f_m=67$ Hz, $A \approx 0.002$ mm, 0.250 mm/peck, 15 s drilling time, Drilling 2.5 mm beyond drill flute
7	Length to Diameter L/D	Drilling 1.2 mm dia, 15 mm deep hole	2-flute carbide twist drill	Oil, flood	Nickel alloy Hastelloy [®] 625	2040 RPM ($f_w=34$ Hz), 0.020 mm/rev, Depth < 2 mm $L/D \sim 1.5$	$f_m=102$ Hz, $A \approx 0.015$ mm, Depth > 10 mm, $L/D \sim 6.5$
8	Tool Wear	Cylindrical turning	Single-point CBN	Oil, mist	Compact Graphite Iron	550 m/min, 1500 RPM ($f_w=25$ Hz), 0.050 mm/rev, 1 mm depth of cut, Tool life < 3 min	$f_m=112.5$ Hz, $A \approx 0.030$ mm, Tool life > 20 min

machining condition. This significant increase in tool life is also notable in that the peck cycle used in the baseline machining was also eliminated with MAM. A peck cycle is the periodic retraction (followed by re-engagement) of a tool, in this case the drill, from the machining zone to enable evacuation of the chips and disruption of the tool–chip contact. It is often found necessary in practice to employ peck cycles in challenging drilling operations, e.g., deep-drilling ($L/D > 8$), drilling work materials of poor workability, to actually accomplish the hole-making. A peck-drilling operation is undesirable since no machining takes place during this period (idle time) and the pecking increases the production cycle time quite substantially. Another example of elimination of a peck cycle, in this case with concomitant, significant reduction in cycle time, is given in Test 5. In this case the work material was a copper alloy, quite difficult to machine because of its ductility. Test 6 illustrates a situation where by employing MAM, the drilling could be carried out over and beyond the length of the drill flute. Typically a drill will fail in such a situation, as it did in the present case in the baseline machining operation, because the long chips flowing up the flutes from the machining zone can no longer be ejected out beyond the flute length and the chips bind the drill causing failure. MAM was successful in this type of test due to the formation of small, discrete chips which could be accommodated inside the drill flutes and ejected after the drill was finally extracted from the hole. In an almost similar vein, Test 7 shows the capability of MAM to drill an extended length ($L/D \sim 6.5$) in Hastelloy[®] that was not possible at the baseline machining condition. A detailed analysis of these tests showed that in all cases the ability to effect discrete chip formation, and disruption of the chip–tool contact enhancing fluid action, were the principal reasons for the success of MAM. Test 8, where disruption of the severe tool–chip contact results in a

dramatic reduction in thermo-chemical wear, is considered in the next section.

6. Enhancing capability by disruption of tool–chip contact

Disruption of the severe tool–chip contact in MAM offers scope for enhancing the life of tools through reduction of wear, especially those dominated by thermo-chemical mechanisms. This possibility was explored with a model system involving continuous turning of compact graphite iron (CGI) with cubic boron nitride (CBN) tools at high speeds (~ 550 m/min). This system was selected because CBN tool life here is known to be determined by thermo-chemical interactions between the tool and the chip [10,23], and machining of CGI with economically-viable tool life has emerged as a major barrier for the use of this material in diesel engine block applications [24].

CGI belongs to the family of cast irons that includes gray cast iron and ductile iron, the principal differences among these irons being in the graphite morphology and chemical composition (e.g., sulfur). Gray cast iron is characterized by randomly-oriented graphite flakes and ductile iron by spheroidal graphite particles. In contrast, the graphite in CGI is often described as vermicular and connected together in a 3-D coral-like network [10]. CGI has much higher strength and stiffness than gray iron, and better damping properties and castability compared to ductile iron. CGI has emerged as a candidate material for diesel engine cylinder blocks based on factors such as strength-to-weight and stiffness-to-weight. However, in order to achieve the graphite morphology, the sulfur content in CGI is kept much lower than in gray iron. This prevents the formation of a manganese sulfide layer at the

tool–chip contact when machining CGI at industrial cutting speeds. Since such a MnS layer is known to facilitate lubrication, besides acting as a diffusion barrier at elevated temperatures, such as those prevailing in the cutting zone, its lack of occurrence at the chip–tool contact with CGI has been cited as a reason for increased ‘thermo-chemical’ wear of CBN tools [10,23]. In addition, the elevated contact temperatures accelerate thermo-chemical wear specific to the iron-CBN system [10,23]. Because CGI is much more ductile than gray cast iron, chip formation with CGI is more continuous, resulting in a tool–chip contact condition more akin to that observed when machining ductile alloys. While much still remains to be resolved about the nature of the thermo-chemical wear mechanisms and contact conditions with CGI, it will suffice to note here that thermo-chemical wear in general should be reduced by lowering the contact temperature and intimacy of tool–chip contact, and promoting conditions conducive for fluid action along the contact. Since MAM conditions of discrete chip formation can accomplish all of these, a significant opportunity has emerged for cost-effective machining of CGI, thereby eliminating potential barriers related to the manufacturability of CGI products using CBN cutting tools.

To determine what effect MAM has on tool wear in the CBN–CGI system, a series of experiments was carried out with a single-point turning configuration in CGI cylinder liners at high speeds (~ 550 m/min) with and without the application of modulation in the presence of an air-mist lubrication (MOBIL VACMUL O3D). The modulation was controlled using a large-scale, prototype modulation device (M4 Sciences LLC) configured to hold a 19.05 mm diameter boring bar used to machine the diameter of the cylinder liners. The machining and modulation conditions for this experimental series can be found under Test 8 in Table 1 and reflect conditions of interest to the industrial sector. A maximum flank wear criterion, $VB_{max}=0.6$ mm, where VB is the usual flank wear land height, was used to define the tool life. It was found, based on several repeatability tests, that the tool life in MAM is at least one order of magnitude greater than in the baseline machining (Table 1, Test 8). The typical evolution of VB_{max} with time, as recorded in one of these tests, is shown in Fig. 8. The tool wear is initially rapid in both the baseline and MAM tests; this is, most likely, a period of ‘running in’ where tool-workpiece conformity is established. After this initial rapid wear, the flank wear during MAM progresses only at a small steady rate, whereas the tool-life criterion ($VB_{max}=0.6$ mm) in the baseline machining is reached rapidly, typically in less than 3 min at this cutting condition. In fact, within about 4 min of testing, the wear land

breached the CBN layer, entering the underlying carbide substrate at a depth of ~ 0.7 mm and destroying the integrity of the cutting edge. In contrast, the flank wear land never reached the tool life limit in any of the MAM tests even after ~ 25 min of cutting, at which stage these tests were stopped.

The modulation frequency in the MAM experiments was $f_m=112.5$ Hz, giving an f_m/f_w ratio of 4.5 for the series (Test 8); consequently, the tool–chip contact was disrupted at least 4 times per second. Visual observations indicated that the chips formed in MAM were much smaller and the temperature of the chip was much lower (based on color) than in the baseline machining condition. A dense smoke cloud was also observed in the vicinity of the machine tool in the baseline machining but not in the MAM, translating the temperature changes into quite a dramatic visual effect. While measurements of the temperature in the cutting region are envisaged in the near future, it should be noted that calculations of machining temperature suggest a significant reduction for the case of MAM [25], consistent with the qualitative observations made herein.

The reduction in CBN tool wear in the presence of modulation is undoubtedly a consequence of the discrete chip formation conditions disrupting the tool–chip contact. A plausible hypothesis as to the mechanism of wear reduction is that the disruption enables a very thin layer of fluid to be active in the contact zone so that the tool wear rate is now primarily determined by the relative hardness of the two bodies in contact, as in many sliding contact situations. Since CBN is much harder than the CGI, the wear rate of CBN should then be small. The likely reduction in contact temperature should also facilitate fluid action and reduce the wear. While this hypothesis needs to be tested, it has been observed in high speed photography with a model cutting system that MAM facilitates fluid access to the cutting zone in a manner akin to that seen with the velocity modulation (Fig. 1c–f). The regular disruption of the contact between the tool and the workpiece created by MAM may indeed alter the thermo-chemical interactions in the CBN–CGI system, enabling access to economically-viable machining solutions.

7. Other implications

The motion control effecting discrete chip formation in MAM has additional implications pertaining to energy efficiency in machining, surface texturing, chip management and recycling/re-use, and powder particulate manufacturing.

7.1. Energy reduction in machining

In discussing the chip formation, the focus thus far has been on the geometric-mechanics aspects of the modulation, such as discrete chip formation and disruption of the tool–chip contact, without consideration of the deformation aspects of the material removal. It is well known, however, that energy consumption in machining is determined by the plastic deformation underlying chip formation, as well as the friction dissipation at the tool–chip contact. So the question arises as to the role of modulation in influencing the plastic dissipation involved in chip formation. In preliminary results reported elsewhere [18], the plastic strain in the discrete chips created by MAM, as inferred from chip thickness ratio measurements, was found to be nearly 40 percent smaller than at the comparable baseline machining condition. Additional evidence for this reduction in strain came from transmission electron microscope characterization of chip microstructures. To investigate this effect further, a finite element (FE) analysis was used to analyze the chip strains in MAM, assuming a perfectly plastic material model for the workpiece. Preliminary

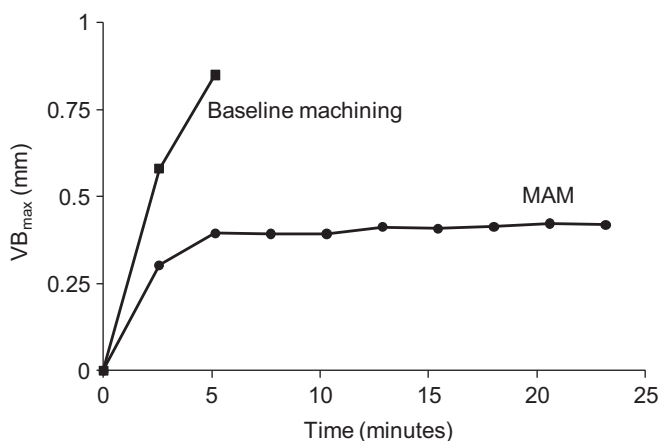


Fig. 8. Variation of maximum flank wear land height (VB_{max}) with time in machining of CGI with CBN. In the baseline machining, the tool life is less than 3 min while in MAM, the tool life is greater than ~ 25 min.

results from this analysis are shown in the strain distribution of Fig. 9 for a MAM condition resulting in a discrete chip. Disregarding the secondary deformation zone adjoining the tool–chip contact, the strain in the chip is seen to be non-uniform and composed broadly of two distinct regions—low and high strain. Even in the higher strain region, the strain values are ~40 percent less than in conventional machining under otherwise identical conditions and similar to that inferred from the experiments [18]. The non-uniformity in the strain is indicative of chip formation occurring in a ‘transient mode’ and consistent with chip microstructures showing a mixture of sub-micron sized and micron-sized grains (ultrafine-grained) at the higher modulation frequencies. In contrast, chips produced in conventional machining showed a homogeneous, refined microstructure consistent with the uniform strain levels recorded therein [26].

These observations highlight an interesting aspect pertaining to the transient nature of deformation in MAM that could potentially be exploited for improving energy efficiency. A combination of measurements and analyses planned in the near future, including direct force/power measurements in MAM should suggest optimum modulation conditions for reducing energy dissipation in machining processes.

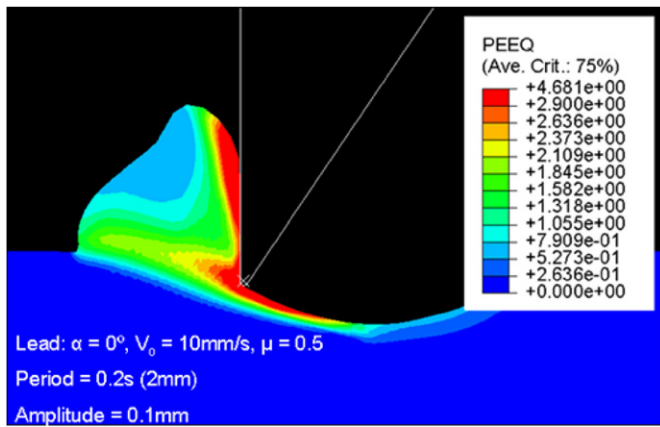


Fig. 9. Finite element analysis results of von Mises effective strain during chip formation by MAM. $f_m=5$ Hz, $A=0.1$ mm, linear 2-D cutting with $V=10$ mm/s. Note the non-uniformity of the strain in the chip.

7.2. Surface texturing

From the discussion pertaining to chip formation in MAM (Eqs. (1)–(4)), it is clear that the modulation offers additional degrees of freedom for controlling the tool motion. This makes it feasible to control the texture (3-D topography) of surfaces using MAM. To explore this possibility, the tool motion in cylindrical turning with MAM was simulated for a specific tool geometry using Eqs. (1)–(4), with the emphasis now being on calculation of the cylinder surface topography rather than the chip geometry. The calculation was carried out till the cylinder surface reached a steady-state profile. The existence of such a unique steady-state profile was confirmed for a range of typical initial conditions.

Fig. 10 shows the steady-state surface texture for a representative patch of the surface in $\phi - A/h_o$ space for various modulation frequencies. The types of surface textures seen are quite remarkable and difficult to achieve in practice on metal surfaces using material removal processes [27]. A consideration of the tool motion shows that the shapes of the surface features are primarily determined by ϕ and A/h_o . A range of surface textures can be created since modulation amplitude (up to 0.2 mm) and frequency (up to 1000 Hz) can be varied continuously, i.e., essentially infinite resolution, with the piezo-based modulators used in the present study. For reference, the bottom row in the figure shows surfaces created in conventional machining.

Fig. 11 (top row) shows macrographs of actual profiles generated in cylinder turning experiments at select conditions corresponding to conventional machining, MAM with continuous cutting ($f_m/f_w=30$) and MAM with discrete cutting ($f_m/f_w=30.5$). The corresponding profiles obtained from the simulation are shown in the bottom row of the figure. The correlation between the 2 sets of profiles is quite striking, demonstrating the capability of the simulation as a tool to explore surface generation in MAM. Since the functional characteristics (e.g., running in, oil retention, wear) of surfaces are determined at least in part by their texture [27], the ability of MAM to produce a range of surface textures could enable access to a functional domain that was hitherto difficult to create.

7.3. Chip recycling and re-use

Discrete chip formation conditions in MAM result in chips of small, well-defined size which can be much more efficiently

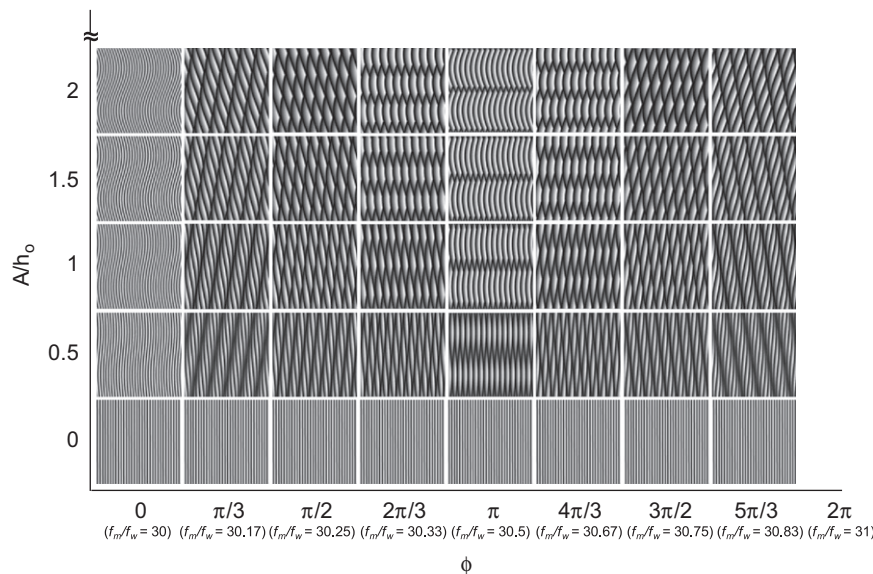


Fig. 10. Surface textures over a 0.6×0.6 mm² surface patch as predicted by simulation of MAM. $h_o=0.01875$ mm (feed/rev, machine setting), depth of cut=0.15 mm, tool nose radius ≈ 0.02 mm, rake angle 0° , lead angle 0° , front relief angle 5° .

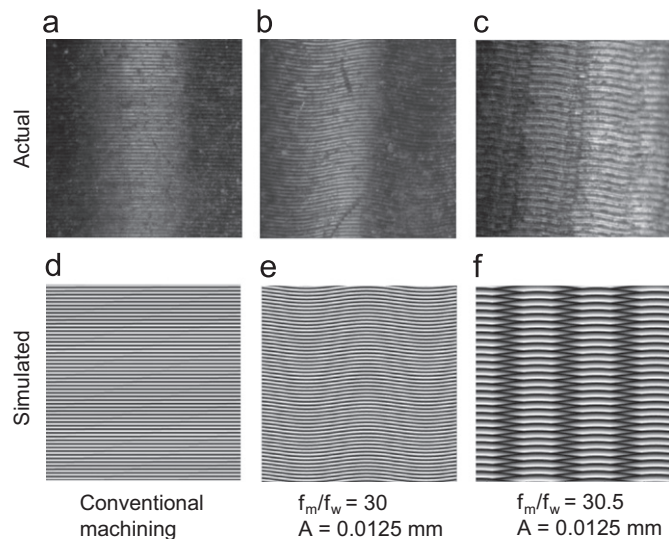


Fig. 11. Surface textures created in conventional cylindrical turning and MAM. The images show a $1 \times 1 \text{ mm}^2$ surface patch with the actual images being optical microscope pictures of surface patches created in experiments. $h_o = 0.01875 \text{ mm}$ (feed/rev, machine setting), depth of cut = 0.15 mm , rake angle 0° , lead angle 0° , front relief angle 5° , tool nose radius is $\approx 0.02 \text{ mm}$. Note the close correspondence between actual surface textures and those predicted by the simulation.

stored, handled and re-processed. Given the large quantities of chips produced as ‘waste streams’ in machining operations across the world, this aspect of MAM offers attractive opportunities for cost-effective chip management and re-use. Furthermore, small chips of controlled size are better suited for consolidation into bulk forms or for use as reinforcements in various matrices (e.g., metals, polymers), creating opportunities for recycling of chip waste streams into higher value products. This is an area attracting increasing attention in recent years due to the large quantities of metal chips produced in industry sectors [28,29]. A recent discovery showing that machining chips can be created in ultra-fine-grained form, with enhanced strength and hardness, has intensified attention in this regard [26,30].

7.4. Particulate production

Control of tool motion can be used to produce chips not only of specific sizes but also of various shapes. This is because chip shape and size are uniquely determined by the combination of machining and modulation conditions. The capability of MAM to produce chips in powder particle form ($\sim 0.020 \text{ mm}$ to several mm) with extraordinary size control, and shapes such as fiber, platelet and equiaxed, from various metal alloy systems (e.g., aluminum and copper alloys, ferrous alloys, and titanium alloys) has already been demonstrated [21,26]. In combination with the simulation capability outlined here, this offers opportunities for developing a class of fiber and powder (materials) manufacturing applications for machining [31].

8. Conclusions

Modulation assisted machining (MAM) can result in the production of small discrete chips when machining ductile alloys, with important changes to the mechanics of machining. The modulation conditions for creating discrete chips have been derived in frequency–amplitude space using a model for MAM. Complementing the chip formation, the texture of the machined surface is influenced by the modulation conditions. These analytical predictions pertaining to chip formation characteristics and

surface texture have been verified over a range of modulation conditions. The model indicates that the conditions resulting in discrete chip formation should also disrupt the severe contact conditions prevailing at the chip–tool interface, facilitating, among other things, fluid action along the contact. The consequences of producing small discrete chips and reducing the severity of the tool–chip contact have been explored using experiments and case studies with drilling and turning. The observations highlight a variety of performance-related benefits of MAM, such as reduction in tool wear, reduction of machining cycle time, controlled surface texturing, smaller energy dissipation and ability to effect machining operations that are difficult, if not impossible, to accomplish without the modulation. The ability to produce small chips of well-defined size offers scope for improved chip management, including recycling and re-use of chips in high-value products. Since MAM can, potentially, be implemented with appropriate equipment modifications on industrial machining systems, exciting opportunities exist for major advances in the capability of machining-based processes.

Acknowledgements

This work was supported in part by NSF grant CMMI-0928337 to Purdue University; NSF grants STTR-IIP-0944980 and SBIR-IIP-0822879 to M4 Sciences LLC, and an NSF Graduate Research Fellowship to C. Saldana.

References

- [1] Shaw MC. Metal cutting principles. Oxford: OUP; 1984.
- [2] Dasch JM, Ang CC, Wong CA, Cheng YT, Weiner AM, Lev LC, et al. A comparison of five categories of carbon-based tool coatings for dry drilling of aluminum. *Surf Coat Technol* 2006;200:2970–7.
- [3] Nakayama K. Studies on the mechanisms of metal cutting. *Bull Fac Eng Yokohama Nat Univ Jpn* 1959;8:1–26.
- [4] Doyle ED, Horne JG, Tabor D. Frictional interactions between chip and rake face in continuous chip formation. *Proc R Soc Lond A Math Phys Sci* 1979;366:173–83.
- [5] Madhavan V, Chandrasekar S, Farris TN. Direct observations of the chip–tool interface in the low speed cutting of pure metals. *J Tribol* 2002;124:617–26.
- [6] De Chiffre L. Mechanics of metal cutting and cutting fluid action. *Int J Mach Tool Des Res* 1977;17:225–34.
- [7] Williams JA, Tabor D. The role of lubricants in machining. *Wear* 1977;43:275–92.
- [8] Huang C, Lee S, Sullivan JP, Chandrasekar S. In situ measurement of fluid film thickness in machining. *Tribol Lett* 2007;28:1:39–44.
- [9] Trent EM. Metal Cutting. 2nd ed.. London: Butterworth; 1984.
- [10] Abele E, Sahm A, Schultz H. Wear mechanism when machining compacted graphite iron. *Ann CIRP* 2002;51(1):53–6.
- [11] Oxley PLB. The Mechanics of Machining. Chichester: Ellis Horwood; 1989.
- [12] Tobias S, Fishwick W. The chatter of lathe tools under orthogonal cutting conditions. *Trans ASME* 1958;80:1079–88.
- [13] Doi S, Kato S. Chatter vibration of lathe tools. *Trans ASME* 1956;78:1127–34.
- [14] Findley H Method and apparatus for cutting material. US Patent 3174404; 1965.
- [15] Kumabe J. Vibration Cutting—Basic Principle and Application. Japan: Jikkyo Shuppan Books; 1979.
- [16] Moscoso W, Olgun E, Compton WD, Chandrasekar S. Effect of low-frequency modulation on lubrication of chip–tool interface in machining. *J Tribol* 2005;127:238–44.
- [17] Chhabra PN, Ackroyd B, Compton WD, Chandrasekar S. Low-frequency modulation-assisted drilling using linear drives. *Proc Inst Mech Eng B: J Eng Manuf* 2002;216:321–30.
- [18] Mann JB, Saldana C, Moscoso W, Compton WD, Chandrasekar S. Effects of controlled modulation on interface tribology and deformation in machining. *Tribol Lett* 2009;35(3):221–7.
- [19] Moriwaki T, Shamoto E. Ultraprecision diamond turning of stainless steel by applying ultrasonic vibration. *Ann CIRP* 1991;40(1):559–62.
- [20] Mann JB, Chandrasekar S, Compton WD. Tool holder assembly and method for modulation-assisted machining. US Patent 7587965; 2009.
- [21] Mann JB, Saldana C, Chandrasekar S, Compton WD, Trumble KP. Metal particulate production by modulation-assisted machining. *Scr Mater* 2007;57(10):909–12.
- [22] Saldana C. Nanostructured particulate by modulation-assisted machining. MS Thesis, Purdue University; 2006.

- [23] Gastel M, Konetschny C, Reuter U, Fasel C, Schulz H, Riedel R, et al. Investigation of the wear mechanism of cubic boron nitride tools used for the machining of compacted graphite iron and grey cast iron. *Int J Refract Metals Hard Mater* 2000;18:287–96.
- [24] Tasdelen B, Escursell M, Grenmyr G, Nyborg L. Machining of gray cast irons and compacted graphite iron. *Swedish Prod Symp* 2007:1–6.
- [25] Kountanya R. Cutting tool temperatures in interrupted cutting—the effect of feed direction modulation. *J Manuf Process* 2008;10:47–55.
- [26] Saldana C, Swaminathan S, Brown TL, Moscoso W, Mann JB, Compton WD, et al. *J Manuf Sci Eng* 2010;132(3):908–20.
- [27] Stout KJ, Davis EJ, Sullivan PJ. *Atlas of Machined Surfaces*. London: Chapman and Hall; 1990.
- [28] Chino Y, Iwasaki H, Mabuchi M. Solid-state recycling for machined chips of iron by hot extrusion and annealing. *J Mater Res* 2004;19:1524–30.
- [29] Uluca Y, Rao BC, Shankar MR, Brown TL, Mann JB, Chandrasekar S, et al. Nanocrystalline materials from aerospace machining chips. SAE Paper No. 2005-01-3306; 2005.
- [30] Brown TL, Swaminathan S, Chandrasekar S, Compton WD, King AH, Trumble KP. Low-cost manufacturing process for nanostructured metals and alloys. *J Mater Res* 2002;17:2484–8.
- [31] Mann JB, Chandrasekar S, Compton WD. Machining method to controllably produce chips with determinable sizes and shapes. US Patent 7628099; 2009.